JOURNAL OF AIRCRAFT
Vol. 31, No. 3, May–June 1994

Calculation of Three-Dimensional Low Reynolds Number Flows

Tuncer Cebeci,* Hsun H. Chen,† and Beng P. Lee‡
California State University, Long Beach, Long Beach, California 90840

An interactive boundary-layer stability-transition approach is used to calculate the performance characteristics of an infinite swept wing at low Reynolds numbers for several angles of attack. The inviscid flow solutions are obtained from an inviscid method based on conformal mapping and the viscous flow solutions from an inverse boundary-layer scheme which uses the Hilbert integral formulation to couple the inviscid and viscous flow. The onset of transition is calculated by the e^n method, based on two- and three-dimensional versions of linear stability theory. Calculated results for an infinite swept wing with an Eppler airfoil cross section are presented for sweep angles corresponding to $\lambda = 30$, 40, and 45 deg, and for Reynolds numbers of 3×10^5 and 4.6×10^5. The effect of sweep angle on lift and drag coefficients is investigated together with the accuracy of predicting the onset of transition with two versions of the e^n method.

Nomenclature

C_d = section drag coefficient
C_l = section lift coefficient
c = chord length
F, f = nondimensional stream functions
G, g = nondimensional functions
L = mixing length or boundary-layer length scale
n = integrated amplification ratio
R = Reynolds number in stability calculations, $u_r L/\nu$
R_c = chordwise Reynolds number, $V_\infty C_s/\nu$
R_x = local Reynolds number, $V_t x/\nu$
u = velocity in x direction
u_r = reference velocity in stability calculations
u_τ = friction velocity
u_0 = reference velocity in boundary-layer calculations
u_∞ = freestream component normal to the leading edge
V_t = total velocity at the edge of the boundary layer, $\sqrt{u_e^2 + w_e^2}$
V_∞ = freestream velocity
v = velocity in y direction
v_n = blowing velocity normal to the surface
w = velocity in z direction
x = Cartesian coordinate normal to the leading edge
y = Cartesian coordinate normal to the surface
z = Cartesian coordinate in spanwise direction
α = angle of attack or normalized wave number
β = normalized wave number
γ_{tr} = intermittency
δ^* = displacement thickness
ε_m = eddy viscosity
λ = sweep angle
ν = kinematic viscosity
ξ = normalized x coordinate, x/c_n
ω = nondimensional frequency

Subscripts

e = boundary-layer edge
i = imaginary quantity
n = normal to the leading edge
s = streamwise
tr = transition
x = x direction

Presented as Paper 91-0187 at the AIAA 29th Aerospace Sciences Meeting, Reno, NV, Jan. 7–10, 1991; received June 3, 1991; revision received Jan. 20, 1993; accepted for publication March 10, 1993.

*Professor and Chair, Aerospace Engineering Department. Fellow AIAA.
†Associate Professor, Aerospace Engineering Department. Associate Fellow AIAA.
‡Graduate Student, Aerospace Engineering Department.

I. Introduction

IN recent years the performance of airfoils operating at chord Reynolds numbers below 5×10^5 has received considerable attention in low-speed aerodynamic flows[1–4] with applications to remotely piloted vehicles, sailplanes, leading-edge control devices, high-altitude vehicles, propellers, and wind turbines. The behavior of these airfoils differs from those at high Reynolds numbers in that the boundary layer remains laminar well into the adverse pressure gradient region, and transition takes place within the separated shear layer prior to reattachment. The resulting separation bubbles can be large in extent and, on airfoils such as the Eppler 387 airfoil,[5] can cover 50% chord of the airfoil at a chord Reynolds number of 1×10^5.

The performance characteristics of airfoils can be predicted by methods based either on the solution of the Navier-Stokes equations or on a combination of inviscid and boundary-layer equations. In both approaches, the accuracy of the method depends on the numerical method, the turbulence model, and the method used to compute the location of transition. The differences between calculation methods for high and low Reynolds numbers are mainly in the prediction of the location of the onset of transition and in the modeling of the transition region. At high Reynolds numbers, the onset of transition occurs before or at the location of flow separation, and the extent of the transition region is confined to a relatively small region. When transition occurs before laminar separation, it can be computed by correlation formulas such as those suggested by Michel[6] and Granville[7] or by the e^n method based on linear stability theory, as suggested by Smith[8] and Van Ingen.[9] Several turbulence models, mostly developed for attached flows, can be used to model the transition region,[10] with those suggested by Dhawan and Narasimha,[11] and Chen and Thyson[12] being popular. Except at very high angles of attack, where the flow corresponds to stall or poststall conditions, these methods and models are often satisfactory in predicting airfoil flows, as discussed in Ref. 13. With decreasing Reynolds number, however, large separation bubbles begin to occur on the airfoil, and the onset of transition may take place inside the bubble and plays a bigger role in the accuracy of the computational method. As a result, the methods used to predict the airfoil characteristics at low Reynolds numbers must be modified to account for those phenomena which are either absent or not important at high Reynolds number flows. In a recent study reported in Ref. 14, the accuracy of a method based on an interactive boundary-layer stability-transition approach developed by Cebeci[15] was in-

vestigated. The inviscid-flow solutions were obtained from a conformal-mapping method and viscous flow solutions from an inverse boundary-layer scheme which made use of a coupling procedure based on a Hilbert integral formulation. The onset of transition was calculated by the e^n method, and the algebraic eddy-viscosity formulation used in the interactive method employed an extended version of the intermittency expression in the Cebeci and Smith eddy-viscosity model.[16] The solution procedure also considered the calculation of flow in the wake, which becomes increasingly important with increased flow separation. Calculated results were presented for the Eppler and Liebeck airfoils with chord Reynolds numbers ranging from 1×10^5 to 5×10^5 and for angles of attack up to stall.[17] Comparison with experiments indicated agreement within measurement uncertainty, except at stall conditions, and close correspondence with the ISES code,[18] which is based on the solution of integral equations.

This article extends the studies of Refs. 14 and 17 on low Reynolds number airfoils to infinite swept wings. Unlike the approach used for airfoil flows, where the solutions of the boundary-layer equations were obtained from the chordwise momentum equation and the location of transition from two-dimensional linear stability theory, the present solutions of the boundary-layer equations are obtained from a combination of chordwise and spanwise components of the momentum equations, and the location of transition is determined with two- and three-dimensional stability theories. This approach is described in the following section and is used to perform calculations for an infinite swept wing with a cross-sectional area corresponding to the Eppler airfoil described in Sec. III. The calculations are performed for three sweep angles and for Reynolds numbers of 3×10^5 and 4.6×10^5 in order to examine the effect the sweep angle has on the lift and drag coefficients at a given angle of attack. In addition, two approaches based on two- and three-dimensional stability and e^n methods are evaluated for computing transition. This article ends with a summary of the more important findings.

II. Calculation Method

The calculation method comprises the interactive boundary-layer method and the stability transition method described below, respectively, operating in an interactive manner.

A. Interactive Boundary-Layer Method

In the extension of the airfoil method[14,17] to the infinite swept wing of Fig. 1, it is assumed that the coordinates of the airfoil are specified by pairs of x/c_s and y/c_s, λ is given, and R_c is defined in terms of streamwise V_∞ and c_s, i.e.

$$R_c = (V_\infty c_s/\nu) \tag{1a}$$

which may be written in terms of c_n as

$$R_c = (V_\infty c_n/\nu)(1/\cos\lambda) \tag{1b}$$

It is also assumed that the wing is sheared so that the streamwise section is unaltered, but the normal chord length is smaller and leads to a higher normal thickness ratio.

The extension of the interactive airfoil method of Ref. 17 to the present infinite swept wing can be accomplished by obtaining the inviscid pressure distribution from a three-dimensional panel method, and the viscous flow solutions from the boundary-layer equations with transition determined from the e^n method for an infinite swept wing based on either two- or three-dimensional stability theory. Since the configuration under examination is an infinite swept wing, the inviscid pressure distributions u_e/V_∞ and w_e/V_∞ needed in the solution of the boundary-layer equations can also be determined from an inviscid method based on conformal mapping for an airfoil cross section in which the y/c_s coordinate is multiplied by $1/\cos\lambda$; and, with $(u_e/u_\infty)_{2d}$ denoting the external two-dimensional velocity distribution corresponding to the modified airfoil cross section, it can be written as

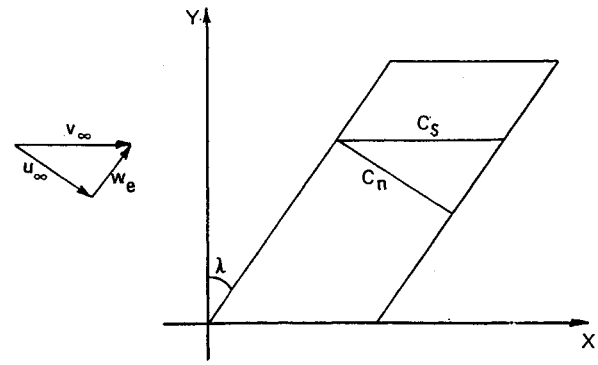

Fig. 1 Notation for infinite swept wing.

$$(u_e/V_\infty) = (u_e/u_\infty)_{2d}\sqrt{1 - \cos^2\alpha \sin^2\lambda} \tag{2a}$$

$$(w_e/V_\infty) = \cos\alpha \sin\lambda \tag{2b}$$

where α denotes the angle of attack and is related to the airfoil angle of attack $(\alpha)_{2d}$ by

$$(\alpha)_{2d} = \tan^{-1}(\tan\alpha/\cos\lambda) \tag{2c}$$

To obtain the viscous flow solutions, the boundary-layer equations are expressed in terms of ε_m, and for a Cartesian coordinate system in which x is normal to the leading edge and z is in the spanwise direction, are written as

$$\frac{\partial u}{\partial x} + \frac{\partial v}{\partial y} = 0 \tag{3}$$

$$u\frac{\partial u}{\partial x} + v\frac{\partial u}{\partial y} = u_e\frac{du_e}{dx} + \frac{\partial}{\partial y}\left[(\nu + \varepsilon_m)\frac{\partial u}{\partial y}\right] \tag{4}$$

$$u\frac{\partial w}{\partial x} + v\frac{\partial w}{\partial y} = \frac{\partial}{\partial y}\left[(\nu + \varepsilon_m)\frac{\partial w}{\partial y}\right] \tag{5}$$

subject to the following boundary conditions for an inverse formulation described in Ref. 19

$$y = 0, \qquad u = v = w = 0 \tag{6a}$$

$$y \to \infty, \qquad u = u_e^0 + \delta u_e(x), \qquad w = w_e^0 \tag{6b}$$

on the wing. Here, u_e^0 and w_e^0 represent the inviscid velocity components in the x and z directions, and $\delta u_e(x)$ is a perturbation velocity computed from the Hilbert integral

$$\delta u_e(x) = \frac{1}{\pi}\int_{x_a}^{x_b}\frac{d}{d\sigma}(u_e\delta_x^*)\frac{d\sigma}{x - \sigma} \tag{7}$$

with the interaction region confined to (x_a, x_b).

To obtain the solutions of the boundary-layer equations in the wake region, with $y = 0$ denoting the dividing streamline in the wake, the chordwise and spanwise momentum equations are solved subject to the following boundary conditions:

$$\begin{aligned} y &= 0, \qquad v = 0 \\ y &= \pm\infty, \qquad u = u_e^0 + \delta u_e(x), \qquad w = w_e^0 \end{aligned} \tag{8}$$

As in two-dimensional flows, v_n is then computed from

$$v_n = \frac{d}{dx}(u_e\delta_x^*) \tag{9a}$$

on the wing and in the wake so that the viscous effects can be introduced into the inviscid method through a nondimensional v_n^* defined by

$$v_n^* \equiv \frac{v_n}{u_\infty} = \frac{v_n}{V_\infty \sqrt{1 - \cos^2\alpha \sin^2\lambda}} \tag{9b}$$

The presence of ε_m requires a turbulence model, and the algebraic eddy-viscosity formulation of Cebeci and Smith, as described in Ref. 16, is used for three-dimensional flows. Thus, the turbulent boundary layer is regarded as a composite layer with inner and outer regions

$$\varepsilon_m = \begin{cases} \varepsilon_{m_i} = L^2 \left[\left(\dfrac{\partial u}{\partial y} \right)^2 + \left(\dfrac{\partial w}{\partial y} \right)^2 \right]^{1/2} \gamma_{tr} & 0 \le y \le y_c \quad (10a) \\ \varepsilon_{m_o} = \alpha_1 \left\{ \displaystyle\int_0^\infty [V_t - (u^2 + w^2)^{1/2}]\, dy \right\} \gamma_{tr} & y_c \le y < \delta \quad (10b) \end{cases}$$

where y_c corresponds to the y location where we switch from the inner eddy-viscosity formula e_{m_i}, to the outer expression e_{m_o}. The parameters in the above equations are given by

$$L = 0.4y[1 - \exp(-y/A)], \qquad A = 26\nu u_\tau^{-1} \tag{10c}$$

$$u_\tau = \nu \left[\left(\frac{\partial u}{\partial y} \right)_w^2 + \left(\frac{\partial w}{\partial y} \right)_w^2 \right]^{1/2} \tag{10d}$$

$$\gamma_{tr} = 1 - \exp\left[-G(x - x_{tr}) \int_{x_{tr}}^{x} \frac{dx}{V_t} \right] \tag{10e}$$

$$G = \left(\frac{3}{C^2} \right) \frac{V_t^3}{\nu^2} R_{x_{tr}}^{-1.34}, \qquad R_x = \frac{V_t x}{\nu} \tag{10f}$$

In Eq. (10f), C is a constant with a recommended value of 60. The expression for G was obtained from data based on two-dimensional attached flows, and in its present form, is not applicable to flows with separation. To take account of separation, a correlation formula described by Cebeci[15]

$$C^2 = 213(\log R_{x_{tr}} - 4.7323) \tag{11}$$

was used to represent C in terms of transition Reynolds number and was based on experimental data with separation-induced transition at low Reynolds number.

Since the boundary-layer equations are parabolic, their solution employs a marching scheme. The similarity variables provide advantages by reducing and even eliminating the growth of boundary-layer thickness $\delta(x)$ and allowing larger steps to be taken in the streamwise direction. For this reason, they are first expressed in transformed variables by introducing the Falkner-Skan transformation in which the similarity variable η is defined by

$$\eta = \sqrt{(u_e/\nu x)}\, y \tag{12a}$$

and the dimensionless variables $f(x, \eta)$ and $g(x, \eta)$ by

$$\psi = \sqrt{u_e \nu x} f(x, \eta), \qquad \phi = \sqrt{u_e \nu x}(w_e/u_e) g(x, \eta) \tag{12b}$$

With this transformation, it can be shown that the boundary-layer equations, Eqs. (3–5), and their boundary conditions for the standard problem where

$$y = 0, \qquad u = v = w = 0$$

$$y = \pm\infty, \qquad u = u_e^0, \qquad w = w_e^0$$

can be expressed as

$$(bf'')' + \frac{m+1}{2} ff'' + m[1 - (f')^2] = \xi \left(f' \frac{\partial f'}{\partial \xi} - f'' \frac{\partial f}{\partial \xi} \right) \tag{13}$$

$$(bg'')' + \frac{m+1}{2} fg'' = \xi \left(f' \frac{\partial g'}{\partial \xi} - g'' \frac{\partial f}{\partial \xi} \right) \tag{14}$$

$$\eta = 0, \qquad f = f' = g = g' = 0 \tag{15a}$$

$$\eta = \eta_e, \qquad f' = g' = 1 \tag{15b}$$

Here, the parameters ξ, b, ε_m^+, f', and g', and the dimensionless pressure gradient parameter m are given by

$$\xi = \frac{x}{c_n}, \qquad b = 1 + \varepsilon_m^+, \qquad \varepsilon_m^+ = \frac{\varepsilon_m}{\nu}, \qquad f' = \frac{u}{u_e}$$
$$g' = \frac{w}{w_e}, \qquad m = \frac{\xi}{u_e} \frac{du_e}{d\xi} \tag{16}$$

Keller's box method is used to solve the above equations by first expressing them as a first-order system. The x-momentum equation, Eq. (13), is written as

$$f' = u \tag{17a}$$

$$u' = v \tag{17b}$$

$$(bv)' + \frac{m+1}{2} fv + m(1 - u^2) = \xi \left(u \frac{\partial u}{\partial \xi} - v \frac{\partial f}{\partial \xi} \right) \tag{17c}$$

and the z-momentum equation, Eq. (14), as

$$g' = s \tag{18a}$$

$$s' = t \tag{18b}$$

$$(bt)' + \frac{m+1}{2} ft = \xi \left(u \frac{\partial s}{\partial \xi} - t \frac{\partial f}{\partial \xi} \right) \tag{18c}$$

subject to the boundary conditions

$$\eta = 0, \qquad f = u = g = s = 0 \tag{19a}$$

$$\eta = \eta_e, \qquad u = s = 1 \tag{19b}$$

The above solution procedure applies to the standard problem in which the external velocity distribution is specified. For flows with separation, the solutions break down at the location of vanishing wall shear and convergence cannot be obtained. This situation can be overcome by using an inverse method in which the external velocity is computed as part of the solution. For this purpose the boundary-layer equations are expressed with variables other than those given by Eq. (12): $u_e(x)$ in Eq. (12) is replaced with u_0, and new dimensionless variables Y, F, and G are defined by

$$Y = \sqrt{u_0/\nu x}\, y, \quad \psi = \sqrt{u_0 \nu x} F(\xi, Y), \quad \phi = \sqrt{u_0 \nu x} G(\xi, Y) \tag{20}$$

so that Eqs. (3–5) can be written as

$$(bF'')' + \frac{1}{2}FF'' + \xi\overline{u_e}\frac{d\overline{u_e}}{d\xi} = \xi\left(F'\frac{\partial F'}{\partial \xi} - F''\frac{\partial F}{\partial \xi}\right) \quad (21)$$

$$(bG'')' + \frac{1}{2}FG'' + \xi\left(F'\frac{\partial G'}{\partial \xi} - G''\frac{\partial F}{\partial \xi}\right) \quad (22)$$

where now

$$F' = \frac{u}{u_0}, \qquad G' = \frac{w}{u_0}, \qquad \overline{u_e} = \frac{u_e}{u_0} \quad (23)$$

Similarly, Eqs. (21) and (22) are expressed as a system of first-order equation as in the standard method. The main difference is that now u_e is unknown and must be computed as part of the solution. Again, the numerical procedure described for the standard method is used to obtain the solution of the above equations subject to the boundary conditions given by Eqs. (6) and (7). For details of the numerical method used to solve the inverse problem, the reader is referred to Ref. 19.

B. Stability Theory and the e^n Method

An important aspect of a calculation method for low Reynolds number flows is the procedure used to predict the onset of transition. Unlike high Reynolds number flows, transition occurs inside the separation bubble with low Reynolds number flows and strongly influences the accuracy of the calculation method. The use of correlation formulas often leads to inconsistent results. On the other hand, the use of the e^n method based on the solution of the Orr-Sommerfeld equation, which in dimensionless form and with primes denoting differentiation with respect to $\bar{y}$, is

$$iR(\alpha\bar{u} + \beta\bar{w} - \omega)(\phi'' - \gamma^2\phi) - iR(\alpha\bar{u}'' + \beta\bar{w}'')\phi = \phi^{iv} - 2\gamma^2\phi'' + \gamma^4\phi \quad (24)$$

where

$$\gamma^2 = \alpha^2 + \beta^2 \quad (25)$$

is an accurate way of determining the onset of transition. According to the e^n method, the stability transition calculations for an airfoil flow with separation are started by obtaining the solutions of the laminar boundary-layer equations with an interactive method such as that described in Refs. 14 and 17. The stability calculations with $\beta = 0$, $\bar{w} = \bar{w}'' = 0$ are initiated at the first x station where the Reynolds number exceeds the critical value established for similar boundary layers. Several dimensional frequencies at different x locations are computed on the lower branch of the neutral stability curve in order to determine the amplification rate $\alpha_i(x)$, so that the onset of transition can be determined by evaluating the integral

$$n = -\int_{x_0}^{x} \alpha_i \, dx \quad (26)$$

for several dimensional frequencies in order to find the critical frequency that leads to the most amplified integrated amplification rate.

The prediction of transition in three-dimensional flows with or without separation is an order of magnitude more difficult than that in two-dimensional flows. The method described by Davis et al.[20] employs a correlation of experimental data based on two-dimensional flows and its accuracy for wings with cross-sections corresponding to low drag airfoils such as the Eppler airfoil requires investigation. Furthermore, this correlation method depends on freestream turbulence which does not account for transition due to crossflow instability, and its use for three-dimensional flows—especially at high Reynolds numbers—may be inappropriate.

In our study, the e^n method is used to calculate transition in three-dimensional flows and to obtain the solutions of the Orr-Sommerfeld equation using the spatial amplification approach which differs from the temporal amplification approach of Malik[21] and the spatial amplification approach of Mack,[22] in that the relationship between the two wave numbers, α and β, is not assumed, but computed from the requirement that $\partial\alpha/\partial\beta$ is real, and this follows from concepts based on group velocity using the saddle-point method. According to this requirement, the wave orientation and growth direction of the disturbance are represented by

$$\left(\frac{\partial\alpha}{\partial\beta}\right)_{\omega,R} = -\tan\theta = -\frac{z}{x} \quad (27)$$

With α and β connected through Eq. (27) and with the disturbance propagating along the ray given by the two terms on the right side of Eq. (27), the onset of transition is obtained by calculating the amplification rates $\Gamma(x)$

$$\Gamma = \alpha_i - \beta_i\left(\frac{\partial\alpha}{\partial\beta}\right)_{\omega,R} \quad (28)$$

and evaluating the integral

$$n = -\int_{x_0}^{x} \Gamma \, dx \quad (29)$$

for several dimensional frequencies determined on a special three-dimensional neutral stability curve called a zarf by Cebeci and Stewartson.[23] Recent studies[24,25] conducted for attached flows on infinite-swept wings and bodies of revolution indicate that this procedure is as accurate as that used for two-dimensional flows, and it is used here together with its two-dimensional counterpart.

III. Results and Discussion

Calculations using the method of the previous section are performed for an infinite swept wing with a cross section corresponding to the Eppler 387 airfoil (see Fig. 2) for which there is extensive airfoil data, obtained by McGhee et al.[5] in the Langley Low-Turbulence Pressure Tunnel (LTPT). The tests were conducted at Mach numbers from 0.03 to 0.13 and at chord Reynolds numbers from 6×10^4 to 4.6×10^5. Lift and pitching-moment data were obtained from airfoil surface pressure measurements and drag data from wake surveys. Oil flow visualization was used to determine laminar-separation and turbulent reattachment locations. Before the results are presented for three-dimensional flows in Sec. III.B, a sample of computed results are presented in Sec. III.A, together with experimental data in order to demonstrate the accuracy of the procedure for two-dimensional flows. For more extensive comparisons of calculated and experimental results, the reader is referred to Ref. 14.

A. Results for Two-Dimensional Flows

The calculations for the Eppler airfoil were performed for chord Reynolds numbers of 3×10^5 and 4.6×10^5 and for angles of attack from 0 deg to the stall angle. For all calculations, the value of n was assumed to be 9.

Figures 3a and 3b show a comparison between the calculated and measured lift and drag coefficients at these two chord Reynolds numbers. As can be seen, the computed values agree remarkably well with experiment for all angles of attack up to stall where the computed lift coefficients begin to deviate from data, indicating higher values than those measured. As discussed in Refs. 13 and 14, this discrepancy is due to the transition-calculation procedure, so that with

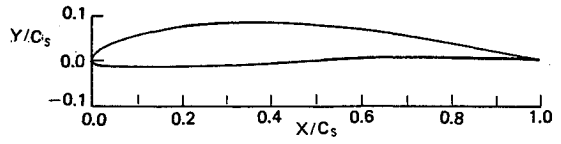

Fig. 2 Eppler 387 airfoil.

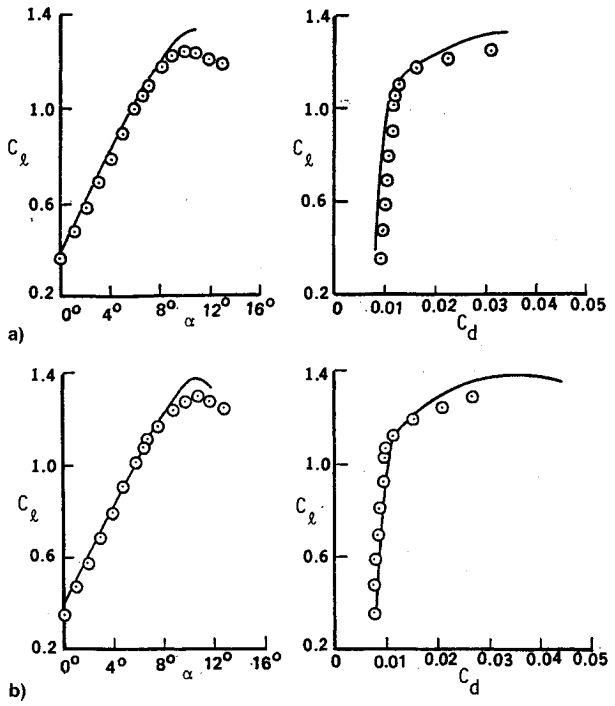

Fig. 3 Comparison of calculated (solid lines) and measured (symbols) lift and drag coefficients for a) $R_c = 3 \times 10^5$ and b) $R_c = 4.6 \times 10^5$.

increasing angles of attack, the onset of transition on the upper surface of the airfoil moves upstream and, near stall conditions, takes place almost at the leading edge. Consistent with the studies of Ref. 13, a very slight change in the transition location has a large effect on the lift and drag coefficients. Moving the transition location downstream increases the region of flow separation, and decreases the lift coefficient in accord with experiment, but, in some cases, it also causes the calculations to break down. To improve the calculations near stall and extend them to poststall flows, it is necessary to implement the present calculation method with procedures similar to those devised for high Reynolds number airfoils, as described in Ref. 26.

Further details of the results corresponding to the calculated values of the chordwise location of laminar separation (LS), turbulent reattachment (TR), the onset of transition, and the lift and drag coefficients are presented in Table 1 for several angles of attack. The experimental results of this table are subject to some uncertainty because of difficulties associated with the surface visualization technique. With this proviso, comparison between measured and calculated values must be considered outstanding. It should be noted that when there is a separation bubble, the transition location obtained from the e^n method occurs within the bubble and, in accord with experimental observation, leads to reattachment some distance downstream.

B. Results for Three-Dimensional Flows

Before the results are presented for three-dimensional flows, similar to those in two-dimensional flows, it is useful to emphasize that the modeling of the transitional region and the onset of transition at low Reynolds numbers are strongly linked through the interactive scheme. If the onset of transition is

Table 1 Experimental and calculated chordwise laminar separation (LS) and turbulent reattachment (TR) and transition locations on the upper surface of the Eppler airfoil together with lift and drag coefficients

Experiment			Calculated				
α, deg	LS	TR	$(x/c)_{tr}$	LS	TR	C_l	C_d
			$R_c = 3 \times 10^5$				
0	0.48	0.69	0.63	0.51	0.72	0.380	0.0078
2	0.45	0.62	0.58	0.46	0.67	0.604	0.0085
4	0.40	0.58	0.52	0.43	0.60	0.825	0.0094
5	0.39	0.55	0.49	0.415	0.57	0.933	0.0099
6	0.38	0.50	0.43	0.42	0.50	1.041	0.0105
			$R_c = 4.6 \times 10^5$				
0	—	—	0.61	0.51	0.68	0.383	0.0066
2	—	—	0.56	0.48	0.62	0.607	0.0071
4	—	—	0.50	0.44	0.55	0.830	0.0079
5	—	—	0.45	0.44	0.49	0.939	0.0085
6	—	—	0.36	—	—	1.044	0.0097

calculated at a position downstream of the true position, even by a small distance, the separation bubble may become numerically unstable. The implication is that laminar flow cannot be sustained to this downstream distance, and the numerical breakdown is indicative of the incorrect location of the onset of transition, as discussed in Ref. 27. Alternatively, the calculation of the correct location of transition together with an improper representation of the subsequent transitional region can lead to a separation bubble length which is incorrect, with consequences for the downstream boundary-layer development.

The comments of the above paragraph have an immediate implication for the present results and the way in which the e^n method and the correlation for γ_{tr}, given by Eqs. (10e), (10f), and (11), are used. This expression for the transitional region in two-dimensional flows was effectively calibrated with experimental data obtained at low Reynolds numbers (see Ref. 15) with $n = 9$ in the e^n method. Its extension to three-dimensional flows requires a similar calibration and corresponding experiments but, since appropriate measurements are not available, the calibration of Eqs. (10e) and (10f) is used here with the velocity representative of the total velocity and retains Eq. (11). With this procedure, a value of n has to be chosen by numerical experiments which corresponds to $n = 7$ in the results presented below.

In the extension of the calculations to an infinite swept wing, it is useful to emphasize the role of Reynolds number and the sweep angle. In the latter case, Eq. (2c) tells us that the angle of attack of the wing (α) and the airfoil (α_{2D}) are related by the sweep angle. For example, Fig. 3b shows that the stall angle for the Eppler airfoil is around 11 deg for $R_c = 4.6 \times 10^5$, which would make the stall angle of the wing around 5.5 deg for a sweep angle of 60 deg. The "true" stall angle, however, is probably lower than this value because the chordwise Reynolds number is equal to $R_c \cos^2\lambda$ or 1.15×10^5 for $\lambda = 60$ deg, and the stall angle for lower Reynolds numbers is smaller.

It is also important to discuss the movement of the transition location with the sweep angle of the wing. Here, there are two features that influence the location of transition. The first results from the increase in airfoil thickness with increase in sweep angle since, in this case c_n is reduced for the same y coordinate. In addition, the angle of attack of the airfoil becomes bigger with an increase in λ [see Eq. (2c)], and this causes the transition location to move upstream. The second feature is the magnitude of the chordwise Reynolds number which becomes smaller with an increase in sweep angle and causes the transition location to move downstream. These two features are in competition with each other, trying to move the location of transition upstream and downstream, respec-

tively. For the case of zero angle of attack, the increase in thickness controls so that the transition location moves upstream with increase in sweep angle.

In the calculations reported here, the onset of transition is obtained from the e^n method with stability calculations performed for three- and two-dimensional flows. It is well known in the former case that crossflow stability becomes increasingly important with an increase in Reynolds number. For example, at chord Reynolds numbers around 2×10^6, with sweep angles corresponding to 50 deg, studies conducted in Ref. 24 show that on an ONERA-wing the location of the critical frequency which leads to the most amplified disturbance and to transition takes place very close to the leading edge of the wing. With low Reynolds number flows, however, we expect the crossflow effect to be small and the disturbances mainly due to Tollmien-Schlichting instabilities, so that the location of the critical frequency occurs downstream of the pressure peak, as in two-dimensional flows. This means that there should be close accord between the predictions of the two versions of the e^n method.

Tables 2 and 3 show the calculated chordwise laminar separation, turbulent reattachment, and transition locations on the upper surface of the Eppler airfoil, together with its lift and drag coefficients as a function of angle of attack for two sweep angles and Reynolds numbers. The calculated results were obtained for a value of $n = 7$, and indicate that, as expected, for both Reynolds numbers the location of transition moves forward with increase in sweep angle at zero angle of attack. For a Reynolds number of 3×10^5, this trend continues up to an angle of attack less than 5 deg, indicating the triumph of the first feature over the second one. At $\alpha =$ 5 deg, transition locations remain the same, but with a further increase in α, the second feature takes over and causes the transition to move slightly downstream with increase in λ. Essentially, the same behavior is observed at the higher Reynolds number, except that the influence of the first feature is limited to lower angles of attack (i.e., $\alpha = 4$ deg) when both features cause the transition location to remain at $(x/c)_{tr} =$ 0.47 at two sweep angles.

An examination of the results in Tables 2 and 3 shows that the total drag coefficients computed from the wake velocity profiles do not change much with sweep angle. For example, at a Reynolds number of 4.6×10^5 and $\alpha = 0$ deg, the drag coefficient decreases by 3% as the sweep angle increases from 30 to 40 deg. However, the lift coefficients decrease substantially with increasing sweep angle. It is to be noted that, as expected, the slope of the lift and angle of incidence curve is almost proportional to cos λ at these angles of attack.

To investigate the effect of sweep angle further on the transition location and on the lift and drag coefficients of the wing, additional calculations were performed for $\lambda = 45$ deg, $R_c = 4.6 \times 10^5$. The results shown in Table 4 indicate the same trend observed at other sweep angles and angles of incidence. For example, at $\alpha = 0$ and 2 deg, transition moves further upstream, but remains at the same location at $\alpha = 4$ and 5 deg. At $\alpha = 6$ deg, the triumph of the second feature continues and pushes the location of transition downstream. The drag coefficients essentially remain unchanged from those at $\lambda = 40$ deg, but the lift coefficients decrease further.

Table 4 also shows the effective angle of attack of the airfoil. As can be seen, with change in wing incidence angle α, the airfoil angle of attack changes quickly and approaches the stall angle of an airfoil typical at these low Reynolds numbers.

Figures 4 and 5 summarize the effect of sweep angle on the lift and drag coefficients and show that, while the drag coefficients essentially remain the same with increase in sweep angle, the lift coefficients decrease as discussed above.

The onset of the transition locations shown in Tables 2–4 were obtained with the three-dimensional version of the e^n method described in Ref. 25. As in two-dimensional flows, the continuation method proved to be very useful and essen-

Table 2 Results for $R_c = 3 \times 10^5$

α, deg	LS	TR	$(x/c)_{tr}$	C_l	C_d
		$\lambda = 30$ deg			
0	0.515	0.67	0.60	0.323	0.0078
2	0.48	0.62	0.55	0.517	0.0084
4	0.43	0.56	0.50	0.718	0.0094
5	0.43	0.51	0.46	0.801	0.0099
6	0.41	0.44	0.41	0.891	0.0107
		$\lambda = 40$ deg			
0	0.500	0.655	0.58	0.282	0.0078
2	0.465	0.605	0.535	0.454	0.0085
4	0.415	0.560	0.490	0.618	0.0095
5	0.395	0.525	0.460	0.698	0.0100
6	0.390	0.470	0.415	0.774	0.0106

Table 3 Results for $R_c = 4.6 \times 10^5$

α, deg	LS	TR	$(x/c)_{tr}$	C_l	C_d
		$\lambda = 30$ deg			
0	0.52	0.63	0.575	0.326	0.0067
2	0.48	0.58	0.53	0.522	0.0071
4	0.46	0.52	0.47	0.714	0.0079
5	0.43	0.46	0.43	0.808	0.0084
6	—	—	0.34	0.896	0.0097
		$\lambda = 40$ deg			
0	0.50	0.63	0.57	0.283	0.0065
2	0.46	0.59	0.525	0.459	0.0072
4	0.425	0.525	0.47	0.628	0.0079
5	0.42	0.485	0.435	0.709	0.0084
6	0.39	0.40	0.375	0.785	0.0093

Table 4 Results for $R_c = 4.6 \times 10^5$ and $\lambda = 45$ deg

α, deg	LS	TR	$(x/c)_{tr}$	C_l	C_d	$(\alpha)_{2D}$
0	0.485	0.63	0.565	0.262	0.0065	0
2	0.45	0.56	0.52	0.421	0.0072	2.83
4	0.41	0.535	0.47	0.574	0.0080	5.65
5	0.40	0.49	0.435	0.647	0.0084	7.05
6	0.39	0.43	0.39	0.714	0.0092	8.45

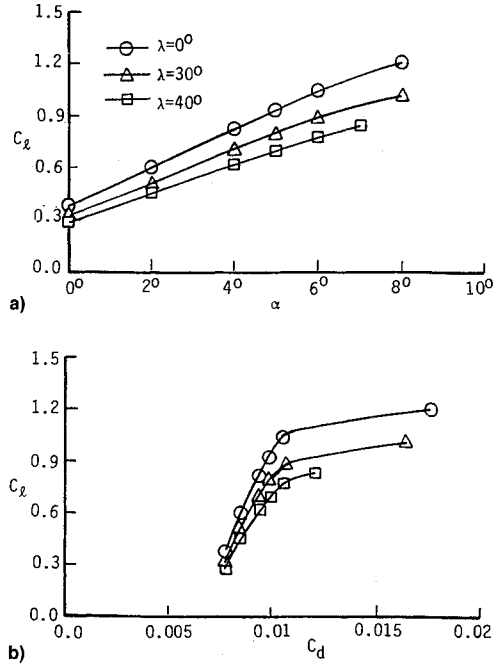

Fig. 4 Effect of sweep angle on lift and drag coefficients at different angles of attack, $R_c = 3 \times 10^5$: a) C_l vs α and b) C_l vs C_d.

tial in computing the eigenvalues in regions of recirculating flow. Additional stability/transition calculations were also performed using the two-dimensional version of the e^n method.[25] In this case, only the solutions of the chordwise momentum equation were examined for transition for $R_c = 4.6 \times 10^5$, $\lambda = 45$ deg. For consistency, again a value of $n = 7$ was used.

Figures 6a and 6b show the variation of n along the airfoil computed with two versions of the e^n method for angles of attack of 0 and 6 deg, respectively. As can be seen, the predictions of both procedures agree well with each other and support the earlier discussion that the effect of crossflow instability becomes increasingly small with a decrease in Reynolds number, and that the disturbances which lead to transition at this Reynolds number are of the Tollmien-Schlichting type.

It is also useful to comment on the influence of the transitional model used in the present eddy-viscosity formulation.

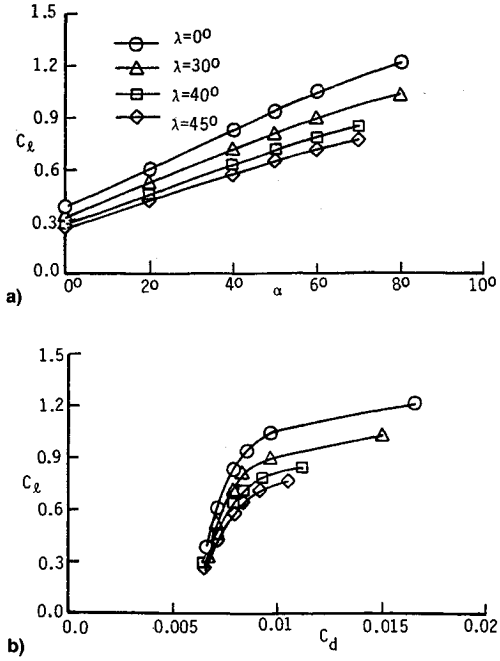

Fig. 5 Effect of sweep angle on lift and drag coefficients at different angles of attack, $R_c = 4.6 \times 10^5$: a) C_l vs α and b) C_l vs C_d.

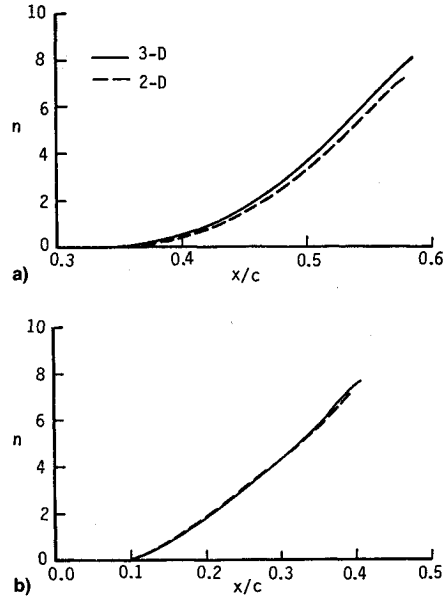

Fig. 6 Variation of n with x/c for $R_c = 4.6 \times 10^5$, $\lambda = 45$ deg: a) $\alpha = 0$ deg and b) $\alpha = 6$ deg.

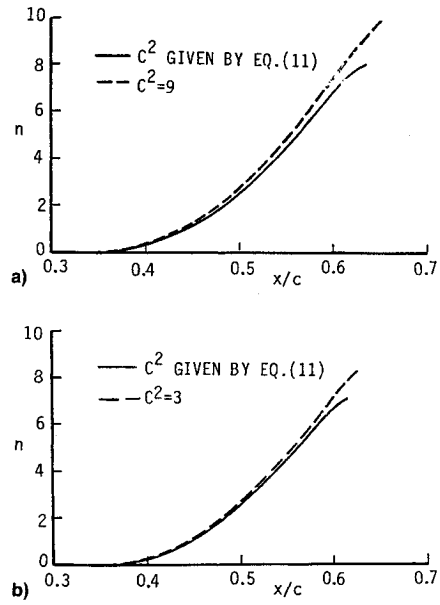

Fig. 7 Influence of C^2 term in Eq. (10f) on the value of n for $R_c = 3 \times 10^5$, $\alpha = 0$ deg: a) $\lambda = 30$ deg and b) $\lambda = 40$ deg.

Our calculations indicated that the location of transition corresponding to $n = 7$ was also the "most" downstream transition location; any attempts of specifying this location more downstream led first to the increase in the extent of the separation bubble, then to the breakdown of the calculations. As a result, the value of n was restricted to 7 for transition calculations. Additional calculations performed with values of C^2 lower than those given by Eq. (11) allowed the transition calculations for higher values of n (see Fig. 7) without leading to any breakdown. This is expected since by decreasing C^2 in Eq. (10f), the extent of the separation-induced transitional region is decreased and the turbulent reattachment point is moved upstream.

IV. Concluding Remarks

A method for predicting the performance characteristics of infinite swept wings at low Reynolds numbers is described. The procedure, as its counterpart for airfoil flows, is again based on a combination of an interactive boundary-layer and stability-transition methods. The results indicate that for chord Reynolds numbers of 3×10^5 and 4.6×10^5, the effect of sweep angle on the drag coefficient of an Eppler airfoil is small. This is not the case for the lift coefficient which decreases substantially with an increase in sweep angle. The stability/transition calculations indicate that crossflow effect is small at these Reynolds numbers and the transition calculations performed with either the three- or two-dimensional versions of the e^n method essentially yield the same results. The results show that the modeling of the transitional region and the onset of transition at low Reynolds numbers are strongly linked through the interactive scheme, and also indicate the need for better transitional models than those available today.

References

[1]Lissaman, P. B. S., "Low-Reynolds-Number Airfoils," *Annual Review of Fluid Mechanics*, Vol. 15, 1983, pp. 223–239.

[2]Mueller, T. J. (ed.), *Proceedings of the Conference on Low Reynolds Number Airfoil Performance*, Univ. of Notre Dame, UNDAS-CP-77B123, South Bend, IN, June 1985.

[3]Mueller, T. J. (ed.), *Proceedings of the Conference on Low Reynolds Number Aerodynamics*, Univ. of Notre Dame, South Bend, IN, June 1989.

[4]*Proceedings of the International Conference on Aerodynamics at Low Reynolds Numbers*, The Royal Aeronautical Society, Oct. 1986.

[5]McGhee, R. J., Jones, G. S., and Jouty, R., "Performance Characteristics from Wind-Tunnel Tests of a Low Reynolds-Number Air-

foil," AIAA Paper 88-0607, Jan. 1988.

[6]Michel, R., "Etude de la Transition sur les Profiles d'Aile," Establisement d'un Critere de Determination de Point de Transition et Calculde la Trainee de Profile Incompressible, ONERA Rept. 1/1578A, 1951.

[7]Granville, P. S., "The Calculation of the Viscous Drag of Bodies of Revolution," David W. Taylor Model Basin, Washington, DC, Rept. 849, 1953.

[8]Smith, A. M. O., and Gamberoni, N., "Transition, Pressure Gradient, and Stability Theory," *Proceedings of the IX International Congress of Applied Mechanics*, Brussels, Belgium, Vol. 4, 1956, pp. 234–244.

[9]Van Ingen, J. L., "A Suggested Semi-Empirical Method for the Calculation of the Boundary-Layer Region," Rept. No. VTH74, Delft, The Netherlands, 1956.

[10]Narasimha, R., and Dey, J., "Transitional Spot Formation Rate in Two-Dimensional Boundary Layers," *Numerical and Physical Aspects of Aerodynamic Flows III*, edited by T. Cebeci, Springer-Verlag, New York, 1986, pp. 57–74.

[11]Dhawan, S., and Narasimha, R., "Some Properties of Boundary-Layer Flow During the Transition from Laminar to Turbulent Motion," *Journal of Fluid Mechanics*, Vol. 3, 1958, pp. 418–436.

[12]Chen, K. K., and Thyson, N. A., "Extension of Emmon's Spot Theory to Flows on Blunt Bodies," *AIAA Journal*, Vol. 9, 1971, pp. 821–825.

[13]Cebeci, T., Clark, R. W., Chang, K. C., Halsey, N. D., and Lee, K., "Airfoils with Separation and the Resulting Wakes," *Journal of Fluid Mechanics*, Vol. 163, 1986, pp. 323–347.

[14]McIlvaine, M., "Prediction of the Performance Characteristics of Airfoils at Low Reynolds Numbers," M.S. Thesis, Aerospace Engineering Dept., California State Univ., Long Beach, CA, May 1990.

[15]Cebeci, T., "Essential Ingredients of a Method for Low Reynolds Number Airfoils," *AIAA Journal*, Vol. 27, No. 12, 1989, pp. 1680–1688.

[16]Cebeci, T., and Smith, A. M. O., *Analysis of Turbulent Boundary Layers*, Academic Press, New York, 1974.

[17]Cebeci, T., McIlvaine, M., Chen, H. H., and Liebeck, R. H., "Calculation of Low Reynolds Number Flows at High Angles of Attack," *Journal of Aircraft*, Vol. 28, No. 4, 1991, pp. 246–252.

[18]Drela, M., and Giles, M. B., "Viscous-Inviscid Analysis of Transonic and Low Reynolds Number Airfoils," *AIAA Journal*, Vol. 25, No. 10, 1987, pp. 1347–1355.

[19]Bradshaw, P., Cebeci, T., and Whitelaw, J. H., *Engineering Calculation Methods for Turbulent Flows*, Academic Press, London, 1981.

[20]Davis, R. L., Carter, J. E., and Reshotko, E., "Analysis of Transitional Separation Bubbles on Infinite Swept Wings," *AIAA Journal*, Vol. 25, No. 3, 1987, pp. 421–427.

[21]Malik, M. R., "COSAL—A Black Box Compressible Stability Analysis Code for Transition Prediction in Three-Dimensional Boundary Layers," NASA CR-165925, 1982.

[22]Mack, L. M., "Stability of Three-Dimensional Boundary Layers on Swept Wings at Transonic Speeds," International Union of Theoretical and Applied Mechanics, Symposium, Transsonicum III, Göttingen, Germany, May 1988.

[23]Cebeci, T., and Stewartson, K., "On Stability and Transition in Three-Dimensional Flows," *AIAA Journal*, Vol. 18, No. 4, 1980, pp. 398–405.

[24]Cebeci, T., Chen, H. H., and Arnal, D., "A Three-Dimensional Linear Stability Approach to Transition on Wings at Incidence," AGARD Symposium on Fluid Dynamics of Three-Dimensional Turbulent Shear Flows and Transition, Cesme, Turkey, Oct. 1988.

[25]Cebeci, T., and Chen, H. H., "Numerical Method for Predicting Transition in Three-Dimensional Flows by Spatial Amplification Theory," *AIAA Journal*, Vol. 30, No. 8, 1992, pp. 1972–1979.

[26]Cebeci, T., Jau, J., Vitiello, D., and Chang, K. C., "Prediction of Post-Stall Flows on Airfoils," *Numerical and Physical Aspects of Aerodynamic Flows IV*, edited by T. Cebeci, Springer-Verlag, Heidelberg, 1990, pp. 93–106.

[27]Cebeci, T., "Numerical Instabilities in the Calculation of Laminar Separation Bubbles and Their Implications," *AIAA Journal*, Vol. 27, No. 5, 1989, pp. 656–658.